Korean J. Chem. Eng., 33(10), 2898-2907 (2016)
DOI: 10.1007/s11814-016-0160-0

pISSN: 0256-1115
eISSN: 1975-7220

Equilibrium kinetic and thermodynamic studies of Cr(VI) adsorption onto a novel adsorbent of *Eucalyptus camaldulensis* waste: Batch and column reactors

Hajira Haroon[*,**], Tayyab Ashfaq[*], Syed Mubashar Hussain Gardazi[*], Tauqir Ali Sherazi[**], Muhammad Ali[**], Naim Rashid[***], and Muhammad Bilal[*,†]**

*Department of Environmental Science, COMSATS Institute of Information Technology, Abbottabad, 22060, KPK, Pakistan
**Department of Chemistry, COMSATS Institute of Information Technology, Abbottabad, 22060, KPK, Pakistan
***Department of Chemical Engineering, COMSATS Institute of Information Technology, Lahore, 54000, Punjab, Pakistan
****Department of Environmental Sciences, University of Haripur, 22620, KPK, Pakistan
(*Received 8 April 2016 • accepted 8 June 2016*)

Abstract−Cr(VI) adsorption onto *Eucalyptus camaldulensis* sawdust (ECS) waste was investigated in batch and column reactors. Various parameters, including the adsorbent dose, pH, initial concentration, particle size, contact time and temperature were optimized. The maximum adsorption capacity (35.58 mg g^{-1}, 71.16%) was achieved at pH 2.0. Data fitted well to Freundlich and Halsey's models (R^2=0.992), indicating the multilayer adsorption of Cr(VI). It obeys the pseudo-second order kinetics. Endothermic and non-spontaneous nature of Cr(VI) adsorption was observed with positive values of changes in enthalpy (9.83 kJ mol^{-1}), and Gibbs-free energy (1.52, 1.38, 1.24, 1.10 and 0.97 kJ mol^{-1}), respectively. In this column study, the breakthrough curve time increased from 670 to 1,270 min by increasing the bed height from 5 to 15 cm, respectively. Column data was found well fitted to bed depth service time model. Adsorption capacity at 60% breakthrough was 2,443.636 mg L^{-1}. The study indicates that ECS waste can be a promising adsorbent for Cr(VI) remediation from industrial effluents.

Keywords: *Eucalyptus camaldulensis*, Chromium (VI), Adsorption Kinetics, Equilibrium Isotherms, Thermodynamics, Column Reactor

INTRODUCTION

Chromium is mainly released from tanneries, metal processing, electroplating, wood preservative, paint and pigment, textile, steel fabrication, dyeing and canning industries [1]. Chromium exists in different oxidation states: Cr(III) and Cr(VI). Although Cr(III) is essential for human nutrition and glucose metabolism, it is also toxic to the physiology of plants at concentration >150 mg L^{-1}. Cr(VI) is 1,000 times more poisonous than Cr(III), and its contamination in water streams poses a serious threat to human and animal health, as it can cause lung cancer, ulcers, nasal septum perforations, and damage to the kidneys. Due to such mutagenic and carcinogenic properties in living tissues, Cr(VI) is declared as the most noxious metal and is included in the priority list of hazardous substances (CERCLA) [2]. Due to the serious hazardous effects of Cr(VI), the permissible limits set by World Health Organization in drinking and inland waters are 0.05 mg L^{-1} and 0.1 mg L^{-1} respectively.

Various methods, such as ion-exchange [3], ultrafiltration, microfiltration [4], reduction [5], catalytic oxidation [6], biological operations [7], photocatalytic reduction and electrocoagulation [8], are in practice for the removal of Cr(VI) from industrial wastewater. However, each one of these processes has a few limitations. Among all these metal ion removal approaches, adsorption is considered as a potential process based upon its efficiency and cost effectiveness [9]. Attempts have been made to explore Cr(VI) adsorption potential of some economical and abundantly available organic wastes [10,11]. Organic wastes give high efficiency, produce less sludge and have regeneration ability [12]. An array of biomaterials like *Caryota urens* inflorescence waste biomass [13], ash gourd (*Benincasa hispida*) peel waste [14], corn stalk [15] and *Eichhornia crassipes* stem [16] have been applied in batch and column studies for the removal of Cr(VI). The presence of different functional groups like carboxyl ($-COO^-$), amine ($-NH_2^-$), amide ($-C(O)NH_2^-$), carbonyl ($-CO^-$), and hydroxyl ($-OH^-$) on the surface of these adsorbents makes them an ideal choice as metal binding agents [17]. Novel adsorbents like carbon nanobiocomposites [18], nanofiber (CNF), graphite felt (GF) composite [19] and hierarchical magnetic carbon nanosheet assemblies [20] have also been used for water treatment.

Adsorption can be performed in both batch and column modes. Fixed bed column adsorption is preferred for industrial application of wastewater treatment. The data obtained from lab scale column study is useful for industrial application [21,22]. Literature shows that researchers mostly work on Cr(VI) removal through batch study; only few studies explore the mechanism of column experiment. Literature review also shows that *Eucalyptus* bark has been used for removal of Cr(VI); however, the use of *Eucalyptus camaldulensis* sawdust (ECS) in batch and column studies is still unexplored. In this study, Cr(VI) adsorption potential of (ECS) waste was explored in both batch and column reactors. It is an evergreen, fast-growing and abundantly available tree in Pakistan. EC saw-

†To whom correspondence should be addressed.
E-mail: mbilal@ciit.net.pk

dust is generated as a waste by-product in the wood industry, which is used as a fuel. The adsorbent was characterized by using FTIR (Fourier transform infrared spectroscopy), XRD (X-ray diffraction), SEM (Scanning electron microscope) and EDX (Energy dispersive X-ray spectroscopy) analyses. Moreover, adsorption isotherms, kinetics and thermodynamic studies were carried out to find the mechanisms of the adsorption process. Bed depth service time (BDST) model was used for the analysis of the breakthrough curve for Cr(VI) adsorption in fixed bed column.

MATERIALS AND METHODS

1. Chemicals and Reagents

Potassium dichromate ($K_2Cr_2O_7$), purchased from Scharlau Chemie Spain, was used to prepare 1,000 ppm stock solution. This stock solution was used for the preparation of subsequent solutions of desired concentration for various experiments. pH of the solutions was adjusted using 0.1 M HCl and 0.1 M NaOH.

2. Preparation of Adsorbents

Five plant waste biomasses, namely *Zea mays* Cob (ZMC), *Agave sisalana* Leaves (ASL), *Nicotiana tabaccum* Stalks (NTS), *Melia azedarach* Sawdust (MAS) and *Eucalyptus camaldulensis* Sawdust (ECS) wastes, were collected from Khyber Pakhtunkhwa Province (KPK), Pakistan. All biomasses were washed thoroughly with deionized water to remove any adhering materials, followed by drying at room temperature for 24 hours. The dried biomasses were then ground and fractionated into different particle sizes (105-420 μm) by using a set of variable pore size sieves, and a particle size of 420 μm was used throughout the experiments. Finally, the biomasses were transferred to air-tight bags and referred to as adsorbents.

3. Batch Adsorption Experiments

In batch adsorption experiments, the adsorbent dosage of 0.05 g was added to 100 mL conical flasks having 50 mL of synthetic Cr(VI) solution of known concentration (50 mg L^{-1}). The flasks were placed in a shaking incubator (WIS-20, Korea), with fuzzy control system, under the set conditions of time, shaking speed (220 rpm) and the temperature (30 °C). The Cr(VI) adsorption potentials of all the five adsorbents were screened for 24 hours. The effect of contact time on adsorption efficiency of ECS adsorbent was investigated for 24 hours. The effect of temperature (30-50 °C), pH (2-7), the amount of adsorbent (0.5-3 g), particle size (105-420 μm) and initial adsorbate concentration (10-150 mg L^{-1}) were also optimized at equilibrium time. The samples were taken out from the shaking incubator at pre-determined time intervals. Afterwards, the adsorbent was passed through 0.45 μm pore size cellulose nitrate filter paper. The filtrate was analyzed for Cr(VI)

Table 1. Equations used for various models

Models	Equation	Parameters
Freundlich	$q_e = K_F C_e^{1/n}$	q_e is the amount of metal adsorbed at equilibrium, C_e is the equilibrium concentration of Cr(VI) in solution phase, K_f indicate the adsorption capacity, and n is the adsorption intensity while both are calculated from the slope and intercept of the Freundlich isotherm
Halsey	$\ln q_e = \frac{1}{n_H}\ln K_H - \frac{1}{n_H}\ln C_e$	K_H and n_H are Halsey's isotherm constants, which are obtained from the slope and intercept of the plot $\ln C_e$ versus $\ln q_e$
Langmuir	$\frac{1}{q_e} = \frac{1}{q_{max}} + \left(\frac{1}{q_{max}K_L}\right)\frac{1}{C_e}$ $R_L = \frac{1}{1+K_L C_0}$	q_e and C_e are stated above, q_{max} is the maximum adsorption capacity which forms a monolayer onto the ECS adsorbent and K_L is the equilibrium constant related affinity of binding sites. R_L is the dimensionless constant, which indicate the favorability of the adsorption process
Pseudo-second order	$\frac{t}{q_t} = \frac{1}{k_2 q_e^2} + \frac{1}{q_e}t$	q_e is mentioned previously, q_t is the amount of adsorbed Cr(VI) at time t (min). K_2 (g mg^{-1} min^{-1}) is the pseudo-second order rate constant. Both were calculated from the slope and intercept of the plot t/q_t versus t
Intra-particle diffusion	$q_t = K_{pi}t^{1/2} + C_i$	Where q_t (mg g^{-1}) is the adsorption capacity at time t. c_i is the boundary-layer thickness and K_{pi} (mg g^{-1} $min^{0.5}$) is the intra-particle diffusion rate constant. K_{pi} and c_i were calculated from the slope and intercept of the plot qt versus $t^{0.5}$
Thermodynamic study	$K_d = \frac{q_e}{C_e}$	K_d is the coefficient of distribution
	$\ln K_d = \frac{\Delta S}{R} - \frac{\Delta H}{RT}$	Changes in enthalpy (ΔH, kJ mol^{-1}) and entropy (ΔS, kJ mol^{-1}) were calculated from the slop and intercept of the Van't Hoff plot. These determine the thermal nature of ECS adsorbent and randomness at solid-solution interface during Cr(VI) adsorption. R is the universal gas constant (8.314 J mol^{-1} K^{-1}), and T is the temperature (K)
	$\Delta G = \Delta H - T\Delta S$	Change in Gibbs free energy (ΔG, kJ mol^{-1}), which determine the spontaneity of the reaction

with an atomic absorption spectrometer (AA 700, Perkin Elmer). Each experiment was performed in triplicate to obtain standardized results. Adsorption of Cr(VI) per unit mass of the ECS adsorbent was calculated by using the mass balance equation Eq. (1):

$$q=(C_o-C_f)\times V/M \quad (1)$$

where q indicates the metal uptake (mg g^{-1}), C_o and C_f indicates the initial and equilibrium Cr(VI) concentrations (mg L^{-1}) before and after adsorption, respectively, V indicates the volume of synthetic solution (mL) and M represents the adsorbent dose (g).

4. Isotherm, Kinetic Models and Thermodynamics

Various isotherms, including Langmuir, Freundlich and Halsey, were applied to the equilibrium Cr(VI) adsorption data. The conformity between model-predicted and experimental values was analyzed on the basis of the coefficient of determination. Moreover, pseudo-second order and intra-particle diffusion kinetic models were applied to explore the mechanism of Cr(VI) adsorption onto the ECS. The corresponding constants and coefficients of correlations of these models were also determined. The exothermic and endothermic nature of the adsorbent, spontaneity and randomness at the solid-solution interface were also investigated through a thermodynamic study. The equations of the aforesaid models are in Table 1.

5. Column Experimentation

Column experiments were conducted in a glass tube having an internal diameter of 2.5 cm and 50 cm height. ECS waste was packed into a glass column to obtain the desired bed height. The bottom and top of the glass column were covered with the layer of a glass wool and glass beads to ensure close packing of adsorbent and to avoid loss of the adsorbent. Column experiments were carried out at room temperature by varying bed height (5, 10, and 15 cm). Cr(VI) solution of 50 mg L^{-1} concentration was pumped downward with a peristaltic pump having flow rate of 10 mL min^{-1}. The pH of the Cr(VI) solution was kept at the optimum value of 2, as obtained from batch study. The effluent was collected at regular time intervals and the residual concentration of Cr(VI) was analyzed.

The effluent volume, V_{ef} (mL) can be calculated by Eq. (2):

$$V_{ef}=Qt_{total} \quad (2)$$

where Q is the flow rate of Cr(VI) solution, which circulates through the column (mL min^{-1}) and t_{total} is the total time (min).

Breakthrough capacity $Q_{0.5}$ at 50% (C_t/C_o=0.5) is adsorption of Cr(VI) (mg g^{-1}) and can be calculated by using Eq. (3):

$$Q_{0.5}=\frac{\left(\begin{array}{c}\text{breakthrough time at (50\%)}\times\text{flow rate}\\ \times\text{inlet concentration}\end{array}\right)}{\text{mass of biosorbent in the bed (g)}} \quad (3)$$

The column adsorption data was analyzed by using the BDST model.

6. Characterization of the Selected Adsorbent

FTIR analysis of ECS was used to reveal the functional groups, which affects the adsorption process. The dried adsorbent (before and after Cr(VI) adsorption) was converted into pallets using KBr and then FTIR spectrum was observed. The X-ray diffraction patterns were determined on an X-Ray diffractometer (Theta-Theta STOE, Germany) with operating conditions at 40 kV and 40 mA. Absolute scan range was 20 °C to 80 °C at a rate of 2.6 degres per minute. Further analysis of the samples involved the X'Pert high score software package (PANalytical B.V. Almelo, Netherland). SEM analyses were used to study the morphology of ECS adsorbent. The samples were mounted on brass stubs using double-sided adhesive tape. SEM images were taken with scanning electron microscope (JSM-5910) at magnification X100 and X700. The photographs were collected at acceleration voltage of 5 kV using the secondary electron detector. The working distance of 25 mm was maintained. The adsorption of Cr(VI) onto the ECS adsorbent was also verified by EDX analysis.

7. Regeneration

ECS of 0.05 g was treated with 50 mg L^{-1} of Cr(VI) solution at the optimum time (120 min), temperature (50 °C) and pH (2). Cr(VI) loaded adsorbent was filtered, dried and transferred into a series of flasks containing 50 mg L^{-1} of potassium hydroxide, sulfuric acid, sodium hydroxide, nitric acid, acetic acid, ethanol, phosphoric acid, hydrochloric acid, acetone, citric acid, methanol, copper sulphate, acetonitrile, ethyl acetate and ferrous sulfate. Saturated adsorbent was then agitated at 220 rpm for three hours with all desorption solutions. The temperature of 30 °C was chosen for desorption experiments; since the adsorption of Cr(VI) on ECS was endothermic, therefore, low temperature may favor the desorption process.

Percentage desorption of Cr(VI) was calculated by using Eq. (4):

$$\%\ \text{desorption}=\left(\frac{\text{amount of Cr(VI) desorbed}}{\text{amount of Cr(VI) adsorbed}}\right)\times 100 \quad (4)$$

8. Statistical Analysis

Cr(VI) adsorption data were collected in triplicate under homogeneous conditions during all the batch experiments. Results were analyzed by one-way analysis of variance (ANOVA) at a significance level of 0.01 using Statistica (version 10).

RESULTS AND DISCUSSION

1. Screening of an Efficient Adsorbent for Cr(VI) Removal

Cr(VI) removal potential of five different bioadsorbents was

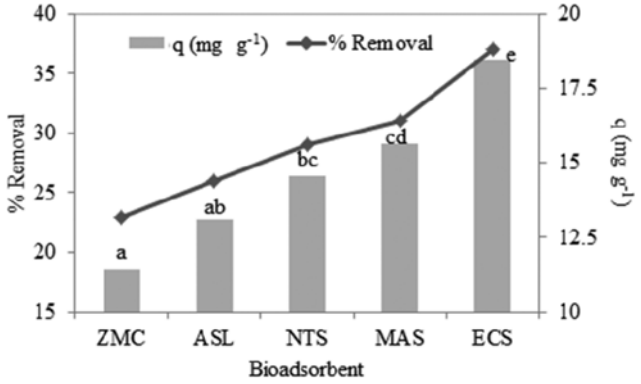

Fig. 1. Cr(VI) removal potential of different bioadsorbents: *Zea mays* Cob (ZMC), *Agave sisalana* Leaves (ASL), *Nicotiana tabaccum* Stalks (NTS), *Melia azedarach* Sawdust (MAS) *and Eucalyptus camaldulensis* Sawdust (ECS). Different alphabets on the error bars represent the mean significant difference at p=0.01.

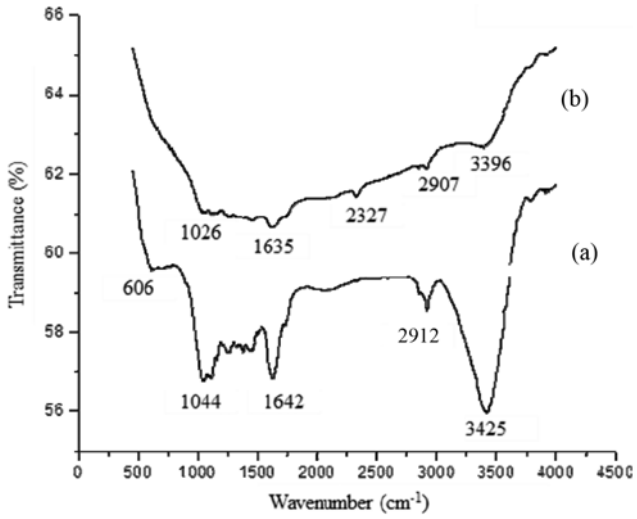

Fig. 2. FTIR spectra of ECS biosorbent before (a) and after (b) Cr(VI) adsorption.

investigated (Fig. 1). ECS showed the significant (p=0.01) high removal of Cr(VI), i.e., 18.5 mg g^{-1}, 37% than MAS (15.6 mg g^{-1}, 31%), NTS (14.5 mg g^{-1}, 30%), ASL (13.1 mg g^{-1}, 26%) and ZMC (11.4 mg g^{-1}, 24%). Therefore, ECS was selected as an efficient biosorbent for Cr(VI) for further experiments. The optimum conditions for Cr(VI) adsorption were investigated through batch adsorption experiments. The presence of functional groups like C-H, Si-O, C=C, C-H and O-H onto ECS surface could be the reason for high Cr(VI) uptake (discussed in Fig. 2), which made this adsorbent a suitable choice for Cr(VI) removal.

2. Characterization of the Bioadsorbent

The surface chemistry, crystalline nature, morphology and elemental composition of ECS bioadsorbent were determined by using FTIR, XRD, SEM and EDX, respectively.

FTIR spectra depict the type of functional groups present on the ECS bioadsorbent surface. The peak at 1,044 cm^{-1} in Fig. 2(a) corresponds to Si-O stretching. The presence of Si was confirmed through EDX analysis of the adsorbent (as discussed in SEM and EDX analysis). The peak at 606 cm^{-1} can be assigned to the bending mode of cellulosic aromatic compounds. The peak at 2,912 cm^{-1} is the characteristic for aliphatic C-H stretching, while the peaks at 3,425 cm^{-1} and 1,642 cm^{-1} are attributed to O-H groups and C=C double bond, respectively. Fig. 2(b) represents FTIR spectrum of adsorbent material after Cr(VI) adsorption, and a change was observed in the four main peaks: 1,044 cm^{-1} to 1,026 cm^{-1}, 1,642 cm^{-1} to 1,635 cm^{-1}, 2,912 cm^{-1} to 2,907 cm^{-1} and 3,425 cm^{-1} to 3,395 cm^{-1} (Fig. 2(b)). This is presumed that the Si-O, C=C double bond, C-H and O-H are the active functional groups, which are involved in the Cr(VI) adsorption process. At low pH, protonation of these functional groups on the adsorbent surface occurs, developing positive charge on the surface, which easily attracts negatively charged chromium ions through electrostatic interaction, consequently, enhanced adsorption. In contrast, at high pH, the reverse may true due to deprotonation phenomenon, which may originate a negatively charged surface, which experiences a repulsive effect to negative chromium ions. For instance, the hydroxyl groups of the adsorbent can be protonated at low pH and then the positively charged groups can interact with the hydrochromate anion ($HCrO_4^-$) and increase the Cr(VI) removal. A similar phenomenon has also been reported elsewhere [23-25].

XRD patterns of ECS bioadsorbent before and after Cr(VI) adsorption are shown in Fig. 3, respectively. XRD spectrum of ECS reflected the amorphous nature and poor crystallinity of the bioadsorbent. The peak at 2θ value of 22.4° shows the presence of cellulose in ECS bioadsorbent before chromium adsorption [26]. The peaks at 2θ values of 44.12° and 64.44° appeared when the adsorbent samples were analyzed after chromium adsorption (Fig. 3). These peaks confirmed the transfer of chromium from solution to ECS biomass. Moreover, these peaks matched the ICSD (inorganic crystalline system data) library, which confirms the presence of chromium oxide specie of Cr_2O_3 at 2θ values of 44.12° (ref. 00-015-0718) with tetragonal crystalline phase and metallic chromium at 2θ values of 64.44° with cubic crystalline phase (ref. 00-001-1250).

SEM depicts the morphology of the adsorbent. It is evident from Fig. 4(a) that the surface of ECS bioadsorbent was rough, uneven, and comprised of heterogeneous pores with a different diameter. The primary pores were observed at 100 μm diameter and magnification of X100, whereas at X700 magnification and 20 μm diameter the secondary pores were observed inside the primary pores onto the ECS adsorbent (Fig. 4(a)). These primary and secondary pores could provide an opportunity for Cr(VI) ions to be sorbed. EDX analysis was carried out for ECS adsorbent before Cr(VI) removal, which indicated the presence of C (53.87%), O (45.35%), Si (0.24%) and Ca (0.54%) on the weight basis, in the structure as shown in Fig. 4(b). In addition, it did not show the signals for Cr in the freshly prepared ECS bioadsorbent. EDX spectrum was also

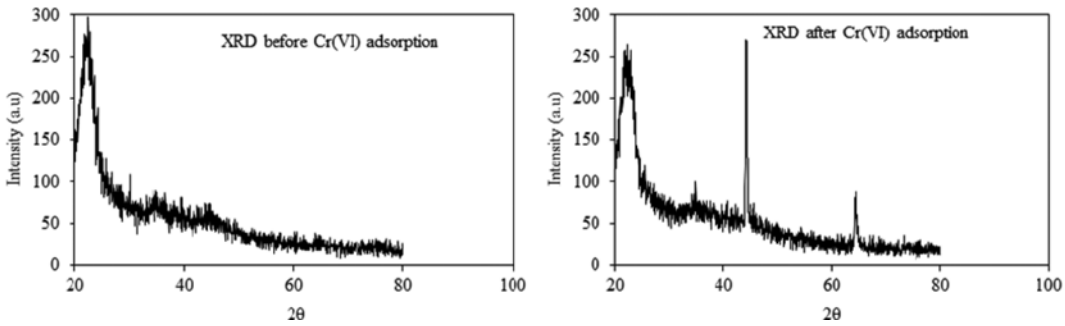

Fig. 3. XRD spectra of ECS.

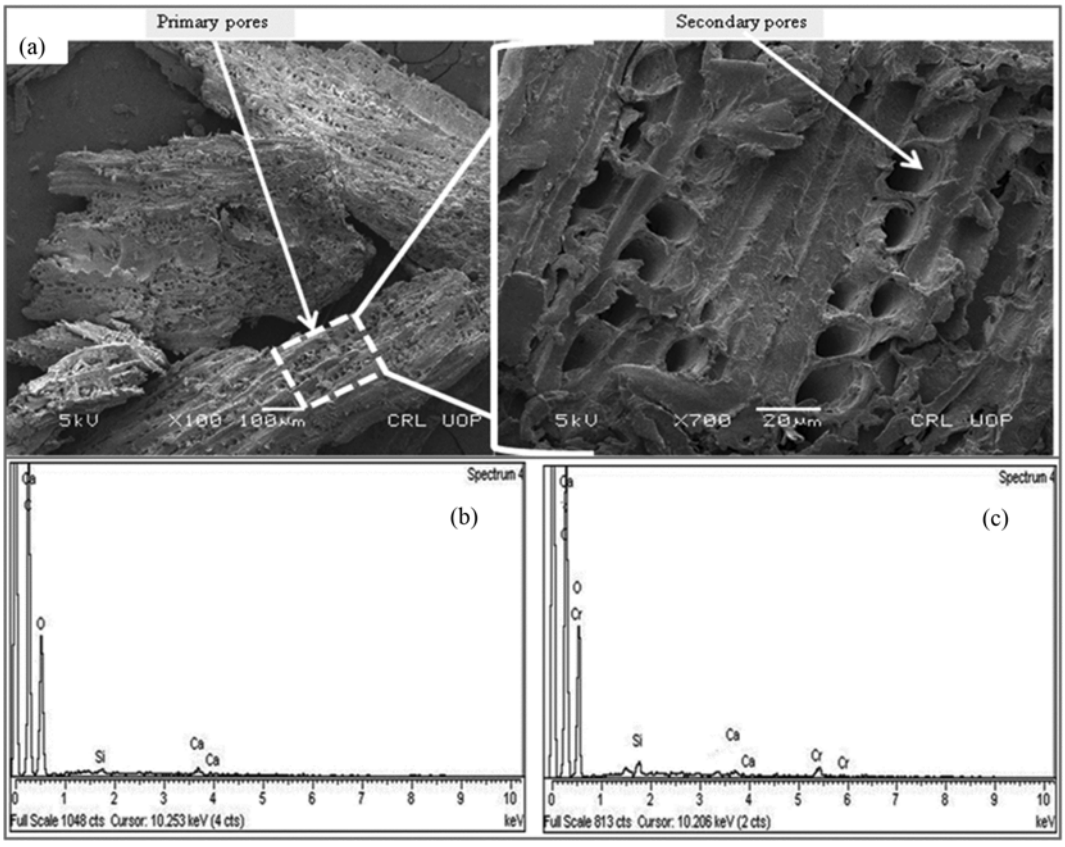

Fig. 4. SEM images of ECS bioadsorbent before Cr(VI) removal (a), EDX spectrum of ECS bioadsorbent before (b), and (c) after Cr(VI) adsorption.

recorded after exposing the 0.05 g ECS biomass with 100 mg L^{-1} Cr(VI) (Fig. 4(b), (c)). EDX spectrum reveals the peaks for Cr at 5.4 KeV and 5.9 KeV energy. It confirms the adherence of Cr(VI) (1.23% by weight) onto the bioadsorbent through the ion-exchange or complexation.

3. Contact Time

The effect of contact time on the adsorption was investigated. Cr(VI) adsorption onto the surface of ECS increased with contact time (Fig. 5(a). The biosorption of Cr(VI) was the highest (14.69 mg g^{-1}, 34.58%) until 120 min. Afterwards there was a negligible effect of contact time on Cr(VI) removal. The reason can be the saturation of active binding sites with Cr(VI) and also the decrease in concentration gradient between the liquid and solid phase. The latter could be the important factor in case of diffusion in secondary pores. Thus, equilibrium time for adsorption of Cr(VI) onto the ECS bioadsorbent was 120 min. So, the rest of the experiments were performed at this contact time.

4. pH

The pH of the aqueous solution is an important factor for metal ion adsorption. It can change the form of Cr(VI) ions, distribution of metal species, the dissociation of functional groups and the adsorbent surface charge. The effects of various pH levels (2-7) were evaluated on the Cr(VI) adsorption capacity and the percentage adsorption (Fig. 5(b)). Cr(VI) exists in aqueous solution in three different ionic forms: dichromate ($Cr_2O_7^{2-}$), chromate (CrO_4^{2-}) and hydrochromate ($HCrO_4^-$). Their stability depends on the pH of solution. At pH 2, the dominant form of Cr(VI) is $HCrO_4^-$, while $Cr_2O_7^{2-}$ ion is present in the range of pH 2-4, and it is present in CrO_4^{2-} form at pH>4. The adsorption capacity and percentage adsorption of Cr(VI) onto ECS was significantly (p=0.01) high (35.58 mg g^{-1}, 71%) at pH 2, than at high pH 7 (24.99 mg g^{-1}, 49.97%), respectively. It shows the preferential adsorption of $HCrO_4^-$ and $Cr_2O_7^{2-}$ ions onto the surface of the ECS adsorbent at pH 2 and 3 respectively. At pH 2, the adsorbent surface becomes positively charged, and thus, it results in the strong electrostatic attraction between $HCrO_4^-$ and adsorbent surface. However, the increase in pH shifts the equilibrium from $HCrO_4^-$ to $Cr_2O_7^{2-}$, and CrO_4^{2-}. At high pH values, OH^- ions compete with the CrO_4^{2-} for active adsorption sites, and consequently the adsorption of chromium is decreased [27]. Similar observations of Cr(VI) ions have also been reported in the literature.

5. Temperature

The adsorption of Cr(VI) onto ECS adsorbent was examined between 30-50 °C. It showed significant (p=0.01) high adsorption capacity of Cr(VI) (20.33 mg g^{-1}, 50%) at 50 °C compare to (17.6 mg g^{-1}, 35%) 30 °C (Fig. 5(c). This reflects the endothermic nature of adsorbent and formation of new adsorption sites, adsorbent and adsorbate chemical interaction or rise in intraparticle diffusion of chromium ions into adsorbent pores at the elevated temperatures. At a high temperature, the breakdown of some internal bonds of the active adsorbent surface and generation of more adsorption sites has been documented in the literature. The move-

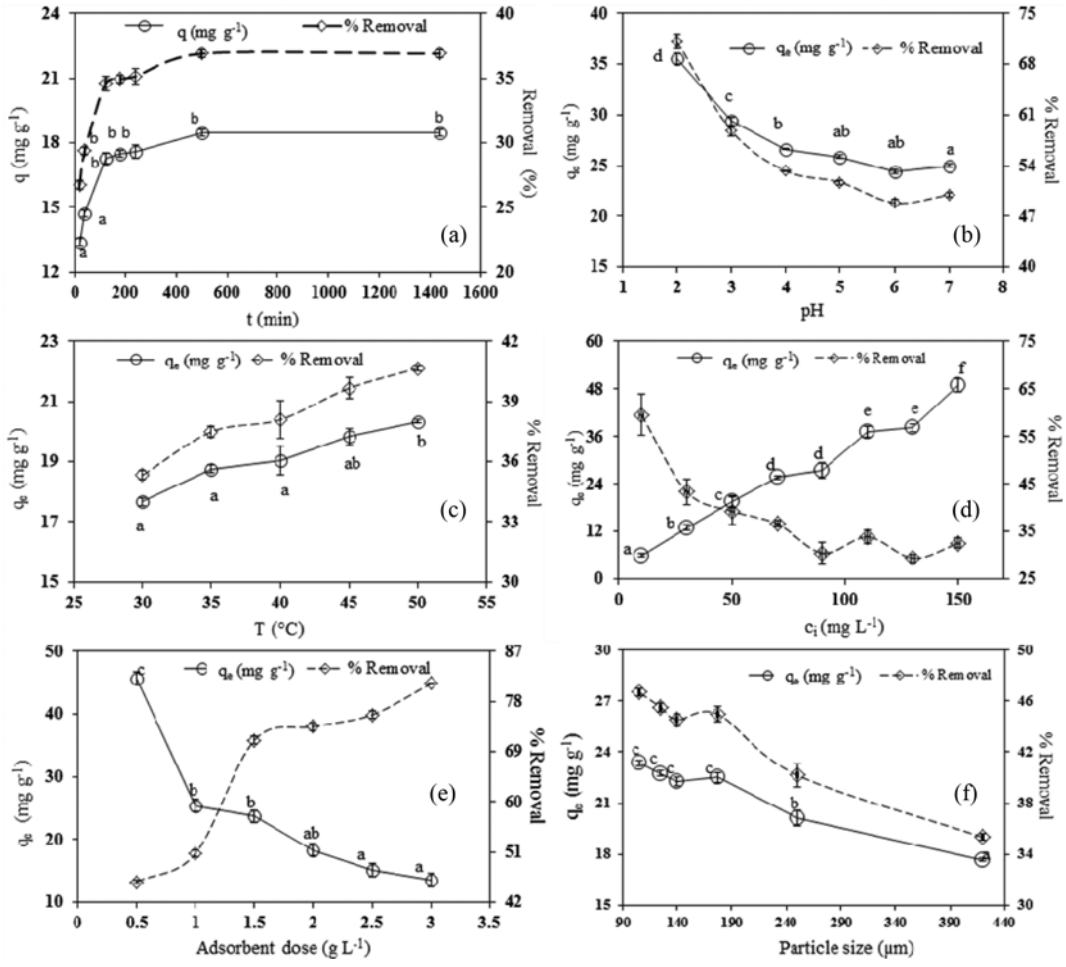

Fig. 5. Effect of contact time (a), pH (b), temperature (c), initial concentration of Cr(VI) (d), adsorbent dose (e), and particle size (f) on Cr(VI) removal capacity of ECS adsorbent.

ment of ions increases at the high temperature, which results in high adsorption [28]. Conversely, the kinetic energy of the metal ions is less at a low temperature, and it is a slow process for Cr ions to reach the adsorbent active binding sites.

6. Initial Adsorbate Concentration

The effect of initial Cr(VI) concentration onto removal efficiency of ECS adsorbent was studied in the range from 10 mg L^{-1} to 150 mg L^{-1}. Data reflected significantly high (p=0.01) Cr(VI) removal from 5.9 mg g^{-1} to 48.8 mg g^{-1} with increasing metal concentration 10 mg L^{-1} to150 mg L^{-1} (Fig. 5(d). It reflects the efficient mass transfer of Cr(VI) from liquid phase to the adsorbent surface driven by the concentration gradient of Cr(VI) and electrostatic interaction [29].

7. Adsorbent Dose

The effect of the various adsorbent doses (0.5 g to 3 g) onto the adsorption capacity of ECS biomass was studied, while keeping other factors (initial concentration of Cr(VI), temperature, pH) constant. Significant high Cr(VI) adsorption capacity (45.7 mg g^{-1}) was observed at ECS adsorbent dose of 0.5 g, whereas the adsorption capacity decreased significantly (p=0.01) with an increase in the bioadsorbent dose (Fig. 5(e)). This is because of the low number of Cr(VI) ions per unit mass of adsorbent, especially when the initial concentration of Cr(VI) is kept constant. However, the percentage removal of Cr(VI) increased from 45.7% to 81% with increasing bioadsorbent doses. This may be the greater surface area or exchangeable sites at high concentration of bioadsorbent [30].

8. Particle Size

Significant (p=0.01) high removal of Cr(VI), *i.e.*, 17.66 mg g^{-1} (35%) to 23.45 mg g^{-1} (46%), was observed when the particle size was reduced from 420 to 105 μm (Fig. 5(f)). This is because of the greater surface area of the smaller particles. The decrease in time required to reach equilibrium was observed with a decrease in the particle size of the adsorbent [28].

9. Isotherm Models

Various isotherm models were used to evaluate the Cr(VI) adsorption capacity of the adsorbents. These models include Freundlich, Halsey and Langmuir. Each model elaborates the particular feature of the adsorption process.

The Freundlich isotherm assumes that adsorption occurs onto a heterogeneous surface of the adsorbent process with stronger binding sites [31-34]. Moreover, increasing adsorption onto binding sites leads to a decrease in the binding strength of the adsorbent. This model shows the best fit to the adsorption data with R^2=0.992 (Fig. S1(a)) compared to the Langmuir isotherm model

Table 2. Langmuir, Freundlich and halsey parameters for Cr(VI) adsorption by ECS bioadsorbent

Isotherm models	Freundlich					Halsey			Langmuir		
Parameters	q_{exp} (mg g^{-1})	q_{max} (mg g^{-1})	1/n	K_F (L g^{-1})	R^2	n_H	K_H	R^2	q_{max} (mg g^{-1})	K_{ads} (L mg^{-1})	R^2
Value	48.83	45.19	0.652	2.23	0.992	−1.53	3.41	0.992	40	0.042	0.967

Table 3. Constants for pseudo-second order and intra-particle diffusion models

Initial Cr(VI) (mg L^{-1})	$q_{e\ exp}$ (mg g^{-1})	Pseudo-second order				Intra-particle diffusion		
		K_2 (g mg^{-1} min^{-1})	$q_{e\ cal}$ (mg g^{-1})	R^2	h (mg g^{-1} min^{-1})	K_p (mg g^{-1} $min^{0.5}$)	c_i (mg g^{-1})	R^2
30	13	0.613	12.12	0.998	90.090	-	-	
50	18	0.002	20.96	0.962	0.6728	-	-	
70	35.8	0.003	37.04	0.997	4.524	0.078	30.07	0.994

(Table 2). The value of 1/n was 0.65, which reflects favorable adsorption [35]. It also shows that the removal of Cr(VI) by ECS adsorbent was multilayer and heterogeneous. K_F (L g^{-1}) value for ECS, as obtained from this work, was 2.23 (Table 2), while the literature shows that K_F (L g^{-1}) values for *Olea europaea* stone, *Cladodes opuntia* biomass, *Solanum tuberosum* peel and *Cocos nucifera* husk are 2.1, 1.642, 0.299 and 0.498, respectively.

The Halsey model is used to assess the multilayer adsorption at a moderately large distance from the surface [36], and its linear form is given in Table 1. The model showed the best fit to the adsorption data with R^2=0.992 (Fig. S1(b), Table 2), which confirmed the heterogeneous nature of the ECS adsorbent.

Langmuir proposed that metal adsorption took place by monolayer adsorption, having energetically homogeneous active sites [33,34,37]. In this process, the metal ions do not migrate in the surface plane. The linear form of the Langmuir model is given in Table 1. Langmuir displays good fit to the equilibrium adsorption data (R^2=0.967) as shown in Fig. S1(c)). A dimensionless constant, R_L (Table 1) was also determined, which may indicate the favorability of the adsorption process. The adsorption process can be described as linear (R_L=1), favorable (0<R_L<1), unfavorable (R_L>1) and irreversible (R_L=0) [30,38-40]. In this study, the value of R_L is 0.19, which supports the suitability of ECS adsorbent for Cr(VI) removal. q_{max} (mg g^{-1}) for ECS is 40 as shown in Table 2, while q_{max} (mg g^{-1}) values for *Olea europaea* stone, *Cladodes opuntia* biomass, *Solanum tuberosum* peel and *Cocos nucifera* husk are 82.51, 18.52, 3.28 and 21.59, respectively [41].

10. Kinetic Models

Different kinetic models, such as pseudo-second order and intra-particle diffusion models, were used to analyze the rate of Cr(VI) removal uptake of ECS adsorbent. The equation of a pseudo second-order model is given in Table 1. A good fit to the experimental data was observed with pseudo-second order model (R^2=0.9973), which reflected that chemisorption was the rate limiting step during the adsorption process (Fig. S2(a)). This involves the exchange or sharing of electrons between adsorbent and adsorbate. Similar observation has been reported in the literature. Moreover, a good agreement was observed between the calculated adsorption capacities and the experimental values at all concentrations (Table 3).

Intra-particle diffusion model is generally used to identify the pathway and mechanism as well as the driving force involved in the adsorption. According to this model, q_t should vary linearly with the square root of time. The general form of this model is given in Table 3. Fig. S2(b) shows that the plot was non-linear over the whole time range. Moreover, the linear potion of the plot is not passing through the origin, which could be due to mass transfer variation at the initial and final stage of adsorption. This dual nature of the linearity reflects that two or more steps of adsorption take place, and diffusion is not the only rate controlling step [42]. It shows that initially the surface adsorption occurs through the boundary-layer diffusion. This way, Cr(VI) moves rapidly from the concentrated solution to the primary pores of the ECS adsorbent as shown in SEM photographs. Finally, the Cr(VI) transports slowly into the secondary pores of the ECS adsorbent (Fig. 3(a)) as the diffusion slows down at equilibrium stage.

11. Thermodynamic Study

All the thermodynamic parameters were calculated from the change of the thermodynamic distribution coefficient (K_d) with a variation of temperature (Table 1). This was further used in the van't Hoff plot. Changes in enthalpy (ΔH) and entropy (ΔS) were calculated from the van't Hoff plot (equation is given in Table 1). ΔH indicated the endothermic nature of the ECS adsorbent with 9.83 kJ mol^{-1}. ΔG was positive at all the temperatures, 303 K, 308 K, 313 K, 318 K and 323 K, with 1.52, 1.38, 1.24, 1.11 and 0.97 kJ mol^{-1}, respectively, which displayed the non-spontaneous reaction. It represents that relatively high temperature supports the Cr(VI) adsorption process. The positive value of entropy (0.03 kJ mol^{-1}) indicated high randomness at the solid-solution interface during the adsorption of Cr(VI) onto the surface of adsorbent.

12. Regeneration

A regeneration study was conducted to reveal the nature of adsorption process, regeneration of adsorbent and recovery of Cr(VI). When metals are easily desorbed by using deionized water, then the adsorption process is physisorption in which metals are loosely bonded onto the adsorbent surface. While in case of strongly bonded chemisorption process, desorption can be done using strong acids

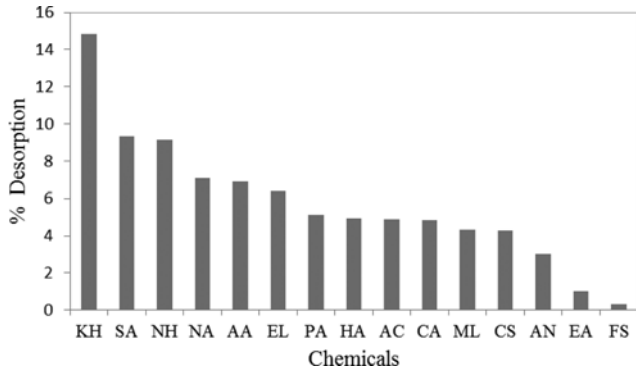

Fig. 6. Regeneration of Cr(VI) from ECS by using 0.1 M solutions of potassium hydroxide (KH), sulphuric acid (SA), sodium hydroxide (NH), nitric acid (NA), acetic acid (AA), ethanol (EL), phosphoric acid (PA), hydrochloric acid (HA), acetone (AN), citric acid (CA), methanol (ML), copper sulphate (CS), acetonitrile (AN), ethyl acetate (EA) and ferrous sulphate (FS).

and bases. Fig. 6 shows that desorption of Cr(VI) was not observed for deionized water, while in case of acids and bases little desorption was observed. The highest desorption of 15% was observed in case of potassium hydroxide. As previously discussed, electrostatic interaction is one of the prominent phenomena responsible for the adsorption process. The use of KH produces an alkaline medium that could weaken the electrostatic interaction between negatively charged chromium ions and adsorbent, promoting the desorption process. However, the incomplete regeneration reflects that few other non-electrostatic processes are also involved in the adsorption process, such as chemisorption, which displays poor regeneration because of the stronger bonds between adsorbate and adsorbent [4].

13. Column Study

A column study was conducted to evaluate the industrial application of adsorbent for the treatment of Cr(VI). The effect of bed height (5 cm, 10 cm and 15 cm) on Cr(VI) adsorption by ECS was investigated at the initial Cr(VI) concentration of 50 mg L^{-1}, flow rate of 10 mL min^{-1} and constant pH of 2. Adsorbent dose affects the adsorption significantly. Fig. 7 shows that breakthrough and

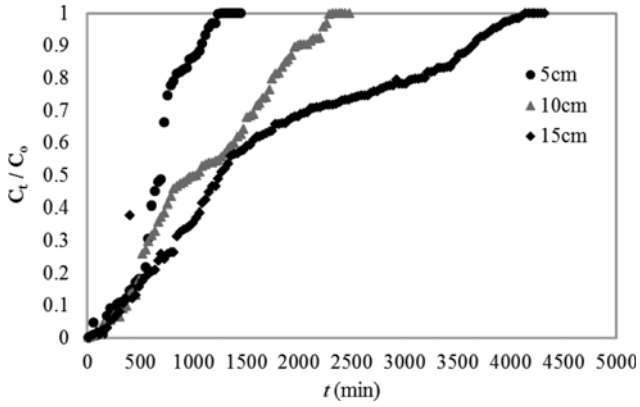

Fig. 7. Break through curve for Cr(VI) adsorption on ECS at different bed heights.

exhaust time increase with an increase in bed height. As the bed height increases from 5-15 cm, the breakthrough (670-1,270 min) and exhaust time (1,240-4,170 min) also increase. This is because available active sites for binding of Cr(VI) are less at small bed height of column. Consequently, the column exhaust time is reached earlier due to the fast saturation rate. Contrarily, the available active sites for Cr(VI) adsorption increase with an increase in column bed height; therefore, the contact time of Cr(VI) with adsorbent also increases, which results in high removal of Cr(VI) [35].

14. Bed Depth Service Time (BDST) Model

Various mathematical models can be used for the analysis of the lab-scale column experiments for the pilot scale design. The BDST model was initially stated by Bohart and Adam (1920) and later modified by Hutchins (1973). This model involves the physical measurement of the adsorption capacity of the bed heights at different values of breakthrough. BDST model is the most applied and the simplest model for heavy metal adsorption in columns. This model is used to predict the relationship between bed depth (Z) and service time (t). This model assumes that adsorption of adsorbate on the adsorbent surface occurs directly, and external mass transfer resistance is negligible [43]. The model is based on the Bohart-Adams equation and can be expressed as follows:

$$t = \frac{NoZ}{CoU} - \frac{1}{KaCo}\ln\left(\frac{Co}{C_b - 1}\right) \tag{5}$$

where t is the service time (min) and z is the bed height (cm). U represents linear velocity of the influent Cr(VI) concentration (cm min^{-1}), N_0 shows adsorption capacity (mg L^{-1}) and K_a is the rate constant (L mg^{-1} min^{-1}). N_0 and K_a can be obtained from the slope and intercept of the plot, respectively, between t and Z. At 50% breakthrough $t=t^{0.5}$, the equation becomes:

$$t^{0.5} = \frac{N_0 Z}{c_0 U} \tag{6}$$

$$t = aZ - b \tag{7}$$

Whereas

$$a = \text{slope} = N_0/C_0U \tag{8}$$

and

$$b = \text{intercept} = \frac{1}{K_a} C_0 \ln\left(\frac{C_o}{C_b} - 1\right) \tag{9}$$

BDST constants are shown in Table 4. BDST constants values are useful to scale up the process with different flow rates and initial concentration of metal without further experimentation. The regression coefficient R^2 values (0.986, 0.979 and 0.955) reflect that data best fits the BDST model. Table 4 shows that with rise in breakthrough (20-60%) the values of slope and adsorption capac-

Table 4. Constants of BDST model for Cr(VI) adsorption onto ECS

c_t/c_0	A	B	N_0 (mg L^{-1})	K_a	R^2
0.2	15	410	381.8182	-0.676241×10^{-5}	0.986
0.4	48	350	1221.818	-2.31694×10^{-5}	0.979
0.6	96	280	2443.636	2.89618×10^{-5}	0.955

ity (N_0) increase from 15 to 96 and 381.82 mg L^{-1} to 2,443.636 mg L^{-1} respectively. At lower breakthrough, some of the active sites on the surface of adsorbent are still unoccupied by Cr(VI), so adsorbent remains unsaturated.

CONCLUSION

Eucalyptus camaldulensis sawdust was evaluated for Cr(VI) adsorption capacity from synthetic solution in batch and column reactors. The maximum removal (71%) was observed at pH 2 in a batch study. Among various isotherms, the Freundlich and Halsey models showed the best fit to the adsorption data with the correlation coefficient value of R^2=0.992, rendering multilayer adsorption characteristics of the ECS biomass. Cr(VI) adsorption by ECS also follows pseudo-second order kinetics, which shows the rate limiting step to be chemisorption. Moreover, the intraparticle diffusion model shows that the diffusion is not the only rate controlling step. Thermodynamic parameters, ΔH (9.83 kJ mol^{-1}), ΔS (0.03 kJ mol^{-1}) and positive ΔG (1.52, 1.38, 1.24, 1.11 and 0.97 kJ mol^{-1}) indicate the endothermic, increased randomness and non-spontaneous nature of adsorption. The maximum regeneration of 15% by potassium hydroxide reveals chemisorption nature of Cr(VI) adsorption on ECS. Lab scale column study reveals that different bed heights have significant effect on performance of column. Best fitted BDST model shows linear relationship between bed height and service time. The results showed that the ECS can be a potential alternative to high-cost adsorbents for the removal of Cr(VI) from the industrial effluents.

ACKNOWLEDGEMENTS

The authors extend their gratitude to the Higher Education Commission of Pakistan for providing funding for the research project (20-1915/R&D/10/5253).

SUPPORTING INFORMATION

Additional information as noted in the text. This information is available via the Internet at http://www.springer.com/chemistry/journal/11814.

REFERENCES

1. E. Demirbas, M. Kobya and A. Konukman, *J. Hazard. Mater.*, **154**, 787 (2008).
2. G. Moussavi and B. Barikbin, *Chem. Eng. J.*, **162**, 893 (2010).
3. L.-C. Lin, J.-K. Li and R.-S. Juang, *Desalination*, **225**, 249 (2008).
4. S. Mandal, M. K. Sahu, A. K. Giri and R. K. Patel, *Environ. Technol.*, **35**, 817 (2014).
5. P. K. Ghosh, *J. Hazard. Mater.*, **171**, 116 (2009).
6. C.-Y. Cao, Z.-M. Cui, C.-Q. Chen, W.-G. Song and W. Cai, *J. Phys. Chem. C*, **114**, 9865 (2010).
7. D. Sivakumar, *Int. J. Environ. Sci. Technol.*, **10**, 903 (2013).
8. C. E. Barrera-Díaz, V. Lugo-Lugo and B. Bilyeu, *J. Hazard. Mater.*, **223**, 1 (2012).
9. M. Bilal, J. A. Shah, T. Ashfaq, S. M. H. Gardazi, A. A. Tahir, A. Pervez, H. Haroon and Q. Mahmood, *J. Hazard. Mater.*, **263**, 322 (2013).
10. V. K. Gupta, A. Nayak and S. Agarwal, *Environ. Eng. Res.*, **20**, 1 (2015).
11. S. Hokkanen, A. Bhatnagar and M. Sillanpää, *Water Res.*, **91**, 156 (2016).
12. D. Sud, G. Mahajan and M. Kaur, *Bioresour. Technol.*, **99**, 6017 (2008).
13. S. Rangabhashiyam and N. Selvaraju, *J. Taiwan Inst. Chem. Eng.*, **47**, 59 (2015).
14. K. Sreenivas, M. Inarkar, S. Gokhale and S. Lele, *J. Environ. Chem. Eng.*, **2**, 455 (2014).
15. S. Chen, Q. Yue, B. Gao, Q. Li, X. Xu and K. Fu, *Bioresour. Technol.*, **113**, 114 (2012).
16. S. Singha, U. Sarkar, S. Mondal and S. Saha, *Desalination*, **297**, 48 (2012).
17. J. L. Barriada, S. Caridad, P. Lodeiro, R. Herrero and M. E. S. de Vicente, *Bioresour. Technol.*, **100**, 1561 (2009).
18. L. R. Varghese, D. Das and N. Das, *Korean J. Chem. Eng.*, **33**, 238 (2016).
19. Y. Shen, L. Li, K. Xiao and J. Xi, *ACS Sustainable Chem. Eng.*, **4**, 2351 (2016).
20. Y. Shen, L. Li and Z. Zhang, *J. Phys. Chem. C.*, **120**, 6659 (2016).
21. S. Baral, N. Das, T. Ramulu, S. Sahoo, S. Das and G. R. Chaudhury, *J. Hazard. Mater.*, **161**, 1427 (2009).
22. M. Calero, F. Hernáinz, G. Blázquez, G. Tenorio and M. Martín-Lara, *J. Hazard. Mater.*, **171**, 886 (2009).
23. A. S. Krishna Kumar, S.-J. Jiang and W.-L. Tseng, *J. Mater. Chem. A*, **3**, 7044 (2015).
24. M. Ilyas, N. Khan and Q. Sultana, *J. Chem. Soc. Pak.*, **36**, 1003 (2014).
25. M. H. Dehghani, M. M. Taher, A. K. Bajpai, B. Heibati, I. Tyagi, M. Asif, S. Agarwal and V. K. Gupta, *Chem. Eng. J.*, **279**, 344 (2015).
26. Y. Tian, M. Wu, X. Lin, P. Huang and Y. Huang, *J. Hazard. Mater.*, **193**, 10 (2011).
27. M. Bhaumik, S. Agarwal, V. K. Gupta and A. Maity, *J. Colloid Interface Sci.*, **470**, 257 (2016).
28. M. Aliabadi, I. Khazaei, H. Fakhraee and M. Mousavian, *Int. J. Environ. Sci. Technol.*, **9**, 319 (2012).
29. U. K. Garg, M. Kaur, V. Garg and D. Sud, *Bioresour. Technol.*, **99**, 1325 (2008).
30. M. H. Dehghani, D. Sanaei, I. Ali and A. Bhatnagar, *J. Mol. Liq.*, **215**, 671 (2016).
31. P. Wang, M. Cao, C. Wang, Y. Ao, J. Hou and J. Qian, *Appl. Surf. Sci.*, **290**, 116 (2014).
32. Y. Bai, D. Lin, F. Wu, Z. Wang and B. Xing, *Chemosphere*, **79**, 362 (2010).
33. K. Wang, G. Qiu, H. Cao and R. Jin, *Materials*, **8**, 8378 (2015).
34. X. Huang, Y. Liu, S. Liu, X. Tan, Y. Ding, G. Zeng, Y. Zhou, M. Zhang, S. Wang and B. Zheng, *RSC Adv.*, **6**, 94 (2016).
35. K. Anbalagan, P. S. Kumar and R. Karthikeyan, *Desalin. Water Treat.*, **57**, 12585 (2015).
36. T. Zhang, Q. Li, Y. Liu, Y. Duan and W. Zhang, *Chem. Eng. J.*, **168**, 665 (2011).
37. L. D. Prola, F. M. Machado, C. P. Bergmann, F. E. de Souza, C. R. Gally, E. C. Lima, M. A. Adebayo, S. L. Dias and T. Calvete, *J. Envi-*

ron. Manage., **130**, 166 (2013).
38. L. Deng, Z. Shi and X. Peng, *RSC Adv.*, **5**, 49791 (2015).
39. M. L. Paul, J. Samuel, S. B. Das, S. Swaroop, N. Chandrasekaran and A. Mukherjee, *Ind. Eng. Chem. Res.*, **51**, 15242 (2012).
40. T. Venkatesha, R. Viswanatha, Y. A. Nayaka and B. Chethana, *Chem. Eng. J.*, **198**, 1 (2012).
41. F. Mutongo, O. Kuipa and P. K. Kuipa, *Bioinorg. Chem. Appl.*, **2014, Article ID 973153**, 7 (2014).
42. E. Haque, J. E. Lee, I. T. Jang, Y. K. Hwang, J.-S. Chang, J. Jegal and S. H. Jhung, *J. Hazard. Mater.*, **181**, 535 (2010).
43. R. Han, D. Ding, Y. Xu, W. Zou, Y. Wang, Y. Li and L. Zou, *Bioresour. Technol.*, **99**, 2938 (2008).

Supporting Information

Equilibrium kinetic and thermodynamic studies of Cr(VI) adsorption onto a novel adsorbent of *Eucalyptus camaldulensis* waste: Batch and column reactors

Hajira Haroon[*,**], Tayyab Ashfaq[*], Syed Mubashar Hussain Gardazi[*], Tauqir Ali Sherazi[**], Muhammad Ali[**], Naim Rashid[***], and Muhammad Bilal[*,†]**

*Department of Environmental Science, COMSATS Institute of Information Technology, Abbottabad, 22060, KPK, Pakistan
**Department of Chemistry, COMSATS Institute of Information Technology, Abbottabad, 22060, KPK, Pakistan
***Department of Chemical Engineering, COMSATS Institute of Information Technology, Lahore, 54000, Punjab, Pakistan
****Department of Environmental Sciences, University of Haripur, 22620, KPK, Pakistan
(*Received 8 April 2016 • accepted 8 June 2016*)

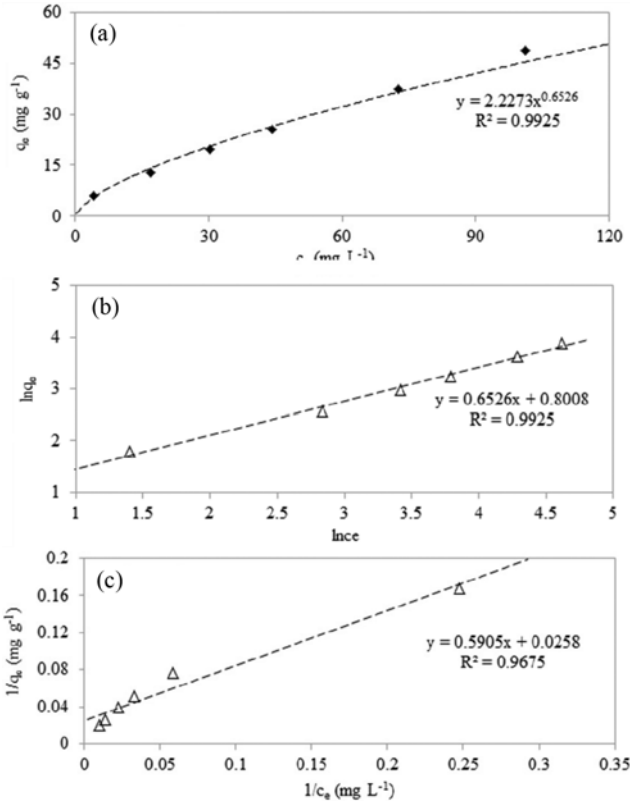

Fig. S1. Plot of (a) Freundlich, (b) Halsey isotherm, (c) Langmuir isotherm.

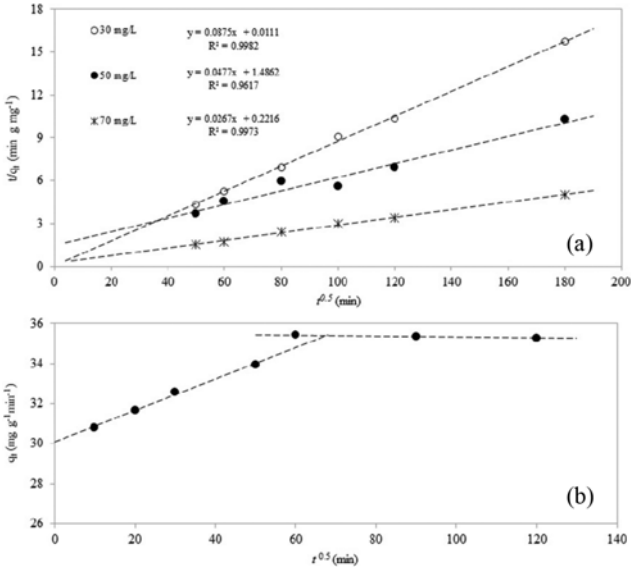

Fig. S2. Pseudo-second order (a), and intra-particle diffusion (b) models for Cr(VI) adsorption onto ECS adsorbent.